J. Fluid Mech. (1990), *vol.* 213, *pp.* 419–442
Printed in Great Britain

Modification of large eddies in turbulent boundary layers

By SHI-ING CHANG AND RON F. BLACKWELDER
Department of Aerospace Engineering, University of Southern California, Los Angeles, CA 90089-1191, USA

(Received 20 January 1989 and in revised form 26 September 1989)

Turbulent boundary layers were altered with a tandem array of manipulators arranged to produce a maximum drag reduction. The Reynolds number based on the momentum thickness, Re_θ, at the first manipulator position was between 1700 and 2400. Temperature was used as a passive contaminant to explore the dynamical relationship between the near-wall and outer regions of the manipulated layer. Heat was introduced by warming the wall uniformly to 15 °C above the ambient temperature or with a line heater in the wake of the manipulator. Temperature and velocity measurements showed a reduction in fluctuation amplitude and a strong decrease in larger scale mixing accompanied by a reduction of the Taylor microscale and integral lengthscale. Isocorrelations indicated that the eddy size was decreased in all three directions. The net result of the manipulators was a marked decrease in the entrainment of irrotational fluid into the boundary layer. The results suggest that the manipulators do not directly affect the wall region but rather decrease the entrainment, and hence the growth of the boundary layer, leading to possible drag reduction.

1. Introduction

Knowledge concerning boundary-layer eddy structures has increased dramatically in the last two decades and the control of turbulent boundary layers, especially their drag, is of considerable interest. Anders (1985) states that a 5% drag reduction on commercial aircraft could promote an overall saving of 400 million dollars per year. This possible benefit has prompted a great deal of research on eddy manipulation. Early studies concentrated on outer-region control owing to the expectation that effects imposed on this region would remain longer than those in the wall region. Recently, thin flat plates parallel to the flow with a streamwise extent of approximately one boundary-layer thickness have been placed in the outer region of the boundary layer. Earlier experimental results have been discussed by Savill & Mumford (1988). These devices were called large-eddy break-up devices (LEBUs) or flow manipulators. Flow visualization showed that the large-scale structures in the outer region of the boundary layer were significantly altered by these manipulators, and anemometer data indicated that the velocity intensities were different as far as 30δ–50δ downstream. Plesniak & Nagib (1985) suggested that a tandem array of thin manipulators in the boundary layer with $h/\delta \approx 0.8$, $l/\delta \approx 1.0$ and $S/\delta = 5$–8 provided an optimum arrangement, where h is the height of the manipulators above the wall, l is their length, S is the streamwise separation between the manipulators and $\bar{U}(\delta) = 0.99U_\infty$. They have shown that although the local skin friction may be

reduced by as much as 20–30%, the net drag reduction was much smaller. In addition, the data had considerable scatter and ranged from a net drag reduction of a few percent to a drag increase. Anders (1985) also attributed these large discrepancies to a great many factors such as different measurement methods, the details of the leading edge of the manipulators, device boundary-layer geometry and the Reynolds-number dependence. More recently, Anders (1989) and Coustols, Cousteix & Belanger (1987) have used airfoil manipulators over a wide range of Reynolds numbers and found a net drag increase.

In the present work, the intent was not to redesign or further optimize these configurations and parameters, but rather to study the dynamic structural differences between the unmanipulated (natural) and manipulated flows via the usage of large-eddy break-up devices. Since the manipulators placed in the outer region alter the drag developed on the wall, they must alter the relationship between these two regions. Thus the main objectives of the present investigation were to determine the apparent charge or reduction of the flow quantities which are modified by the manipulators, and to use the manipulators as a diagnostic tool to understand the physics of the relationship between the large-scale eddies and the bursting phenomenon.

2. Experimental apparatus

To avoid facility-dependent problems, two different closed-circuit wind tunnels were used. The low-turbulence wind tunnel had a test section with cross-sectional area of 60×90 cm and length of 6 m, and is described by Blackwelder & Haritonidis (1983). A $0.6 \times 90 \times 600$ cm flat plate, composed of aluminium for the first 360 cm and Plexiglas for the remaining 240 cm, was installed in the test section. The maximum speed in the test section was 20 m/s and turbulence intensity levels were less than 0.04% at all free-stream velocities over the frequency range of 1 Hz to 10 kHz. The Dryden wind tunnel is described by Schubauer & Skramstad (1948) and Gutmark & Blackwelder (1987). The test section had an octagonal shape, 1.4 m between opposite faces. The turbulence level was 0.13% at 25 m/s over the frequency range of 1 Hz to 10 kHz. In the octagonal test section, a 1.3 cm thick aluminium plate, 550 cm long and 133 cm wide, was mounted horizontally. The pressure gradient along both flat plates was approximately zero.

The test plate in the Dryden wind tunnel could be uniformly heated by 24 heating pads which were glued onto the non-working side of the plate and each was designed to give a maximum heat capacity of 500 W. The wall temperature was controlled by eight variable-voltage transformers. Thirty eight thermistors were embedded in the streamwise and spanwide directions on the same side as the heating pads to monitor the uniformity of the plate temperature which was nominally maintained at 15 K above the free-stream temperature at a tunnel speed of 5 m/s.

Analog signals from the anemometers and pressure transducer were digitized and processed by a Digital Equipment Corporation PDP-11/55 minicomputer. All the signals were sampled at a rate of 0.4 ms per channel, which is about one viscous timescale in the turbulent boundary layer. In order to ensure consistency, each data set was repeated at least twice and consisted of an 80 s data record.

Constant-temperature hot-wire anemometers were used extensively for the velocity measurements and are described by Blackwelder & Kaplan (1976). The hot-wire sensors were operated with an overheat of 33%. Fourteen to sixteen anemometer circuit boards were integrated as a system for multi-channel usage. The constant-

current anemometers used to measure the temperature have been described by Chen & Blackwelder (1978). In the present study, the overheat ratio for a 2.5 μm diameter 10% rhodium–platinum sensor was 0.5%, corresponding to 1 mA current.

A hot-wire rake consisting of ten sensors mounted on ten pairs of jeweller's broaches was used for both the velocity and temperature measurements. Each sensor was 1 mm long and the separation between sensors was 6 mm. A triple wire, formed by one cold wire combined with a $\times$-wire, was constructed in such a way that the distance between the cold wire and the downstream $\times$-wire was less than 1 mm, and the separation between each sensor of the $\times$-wire was about 1 mm. A single hot wire was used to measure velocity profiles and a single cold wire was used to measure the temperature profiles in the boundary layer. All of the sensors used were made of 10% rhodium–platinum wire with a diameter of 2.5 μm and were soft-soldered to the jeweller's broaches. Further details are given by Chang (1987).

3. Experimental procedures and techniques

Prior to the start of the hot-wire calibration, the constant-temperature hot wires were dynamically calibrated using the standard square-wave test. The static calibration for the constant-temperature sensors followed the procedure described by Blackwelder & Haritonidis (1983). Once the calibrations were obtained, the probes were moved to the desired position in the turbulent boundary layer and data were recorded. After taking the data, the probes were returned to their original location in the free stream and were checked for drift. If the velocity drift was greater than $\pm 1.5\%$, the data were discarded and all procedures were repeated.

The $\times$-probe was calibrated in the free stream by pitching the probe at five angles with respect to the free-stream direction, $-25° < \alpha < 25°$, in the (x, y)-plane at five tunnel speeds. Hence, there were 25 pairs of voltage outputs (E_1, E_2) from the two sensors of the $\times$-probe and each voltage pair (E_1, E_2) was related to a known velocity pair (U, V) obtained from the pressure transducer and angle measurement. Using a third- or higher-order polynomial, a set of coefficients was obtained for the following relation:

$$U + b_i V = \sum_{j=0}^{3} c_{ij} E_{ij} \quad (i = 1, 2)$$

by a least-square fit of the calibration data.

To obtain the temperature calibrations, the constant-current anemometers were placed inside the potential cone of a heated jet. A thermistor placed near the sensors was used to obtain the reference temperature. The air flow and temperature were controlled independently by two individual variable-voltage transformers. The voltage outputs of the sensors and thermistor were digitized simultaneously for six heating conditions over the calibration range of 25–50 °C. A first-order least-squares curve was sufficient to fit the data.

When velocity and temperature data are taken simultaneously, the cross-contaminations have to be considered. The velocity contamination of the temperature signal was negligible in the present study. The temperature contamination of the velocity was more important, especially in the streamwise velocity signal. After the $\times$–θ probe was calibrated for velocity in the free stream at temperature T_∞, the probe was placed in the heated jet to calibrate the cold wire. The reference velocity and temperature were provided by a temperature-corrected Pitot tube and a thermistor. At each temperature setting, the probe was pitched through $\pm 15°$ with respect to the flow direction. Six to seven temperature settings were taken

which covered a range up to 20 K above T_∞. Since the angle and speed at each data point were known, the U- and V-velocities could be calculated directly and obtained from the calibration coefficients and compared. It was found that the linearized U-signal deviated monotonically from the imposed U-velocity as the temperature increased. The normal velocity data showed very little change as the temperature varied: therefore, no correction was made in the subsequent measurements. This agreed in general with the findings of Champagne (1978) and Corrsin (1949). It is also reasonable from a geometrical consideration of the probe. Since V is approximately proportional to the difference of the cooling velocity between the two sensors of the $\times$-probe, the temperature effect on V was cancelled out by the subtraction of the cooling velocities of these two sensors.

The time constant of the constant-current anemometers was determined in a manner similar to Antonia, Browne & Chambers (1981). A 1.25 μm diameter wire of 10% rhodium–platinum, used as the source heater, was placed perpendicular to the flow direction and heated by a 100 Hz square-wave electrical signal. The 2.5 μm diameter 10% rhodium–platinum constant-current sensor was placed parallel to it 1 mm downstream. Comparison between the thermal forcing signal of the heater and the output yielded a time constant of 0.4 ms. This agreed well with the usual square-wave perturbation tests and yielded a frequency response of 400 Hz at 5 m/s free-stream velocity.

Conditional sampling and averaging techniques have been used extensively to study turbulent shear flows, especially to investigate the turbulent/non-turbulent interface of mixing layers, boundary layers, etc. In most techniques, the velocity components and their derivatives are used to detect the turbulent zones in the intermittent region. It is less common to find the use of a passive scalar as the detection function (see Antonia, Dahn & Prabhu 1977; Larue 1974). Chen & Blackwelder (1978) used the thermal signal to detect the temperature interface in a slightly heated boundary layer and found that the signal-to-noise ratio in the temperature-marked boundary layer was about three times the value found by Kovasznay, Kibens & Blackwelder (1970) using velocity. In the present study, Chen's (1975) techique was used but modified slightly such that only one threshold level was used. Once the detection method and threshold value were determined, conditional averaging was used to obtain the intermittency, interfacial crossing frequency, the turbulent/non-turbulent zone averages, etc. via the methods described by Kovasznay *et al.* (1970) and Hedley & Keffer (1974*b*).

4. Results and discussion

4.1. *Turbulent-boundary-layer geometry*

The experimental set-up is shown in figure 1. Three-dimensional trips on both plates were placed 45 cm from the leading edge to ensure a fully developed turbulent layer at the manipulator locations. In the low-turbulence tunnel, the first manipulator was located at $x_r = 330$ cm from the leading edge of the flat plate; its location was used as the reference. The boundary-layer thickness, δ_r, at this location was 6.0 cm and Re_θ was 2400. The second manipulator was $6.5\delta_r$ downstream of the first. The downstream distance from the first manipulator is given by $\xi = (x-x_r)/\delta_r$. Both manipulators were constructed of 0.1 mm thick stainless steel strips which were $0.63\delta_r$ wide. These manipulators were kept at a constant height, $h = 0.75\delta_r$, from the wall by two spacers allowing a clear span of 75 cm. The manipulators were placed

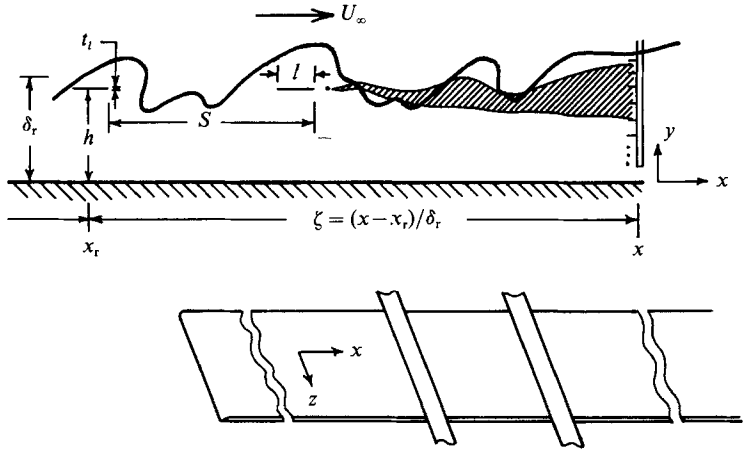

FIGURE 1. Experimental arrangement.

under sufficient tension that no vibration could be found either by a reflected laser beam at a small incidence angle or by the power spectrum measurements of a hot-wire probe placed 1 mm above and below the trailing edge of the manipulator. At lower tension values, vibrations could indeed be induced but were always at a different frequency from the natural shedding of eddies from the manipulators. In addition, vibration yielded as in-phase streamwise velocity component on opposite sides of the wake whereas the naturally shed eddies were 180° out of phase. The manipulators' wake was heated by a 0.125 mm diameter nichrome wire placed 1 mm directly behind the second manipulator. Care was taken to ensure that the heating wire had no direct effect on the velocity field by itself. Without the manipulators installed, the mean and r.m.s. velocity field showed no evidence of the heater at $\xi = 13.2$.

A similar set-up was used in the Dryden wind tunnel except that the direction of gravity was in the positive y-direction, whereas it was in the positive z-direction in the low-turbulence tunnel. The first manipulator was located 170 cm from the leading edge of the flat plate, where δ_r was 3.7 cm and Re_θ was 1700. The non-dimensional geometrical parameters remained identical to those in the low-turbulence wind tunnel. Data from both wind tunnels agreed quite well. Unless otherwise stated in the captions, only the measurements in the Dryden tunnel are presented.

4.2. *Mean and r.m.s. velocity measurements*

The mean velocity profiles, $\bar{U}(y)$, from $\xi = 7.8$ to 71.4 are shown in figure 2 scaled with the local values of u_* and ν. The manipulators' wake is quite evident at $\xi = 7.8$ and 11.9. Note that at $\xi = 71.4$ a small momentum defect still exists compared to the natural flow, indicating that the boundary layer has not fully recovered from the manipulators.

A novel method was utilized to determine the friction velocity, u_*. A least-squares fit of the wall data to Spalding's (1961) law of the wall in the form

$$y^+ = U^+ + e^{-\kappa A}\{e^{\kappa U^+} - 1 - \kappa U^+ - \tfrac{1}{2}(\kappa U^+)^2 - \tfrac{1}{6}(\kappa U^+)^3\}$$

was used, where $U^+ = \bar{U}/u_*$ and $y^+ = yu_*/\nu$. Since κ and A were assumed constant, with values of 0.41 and 5.0, the only remaining unknown parameter was u_* which

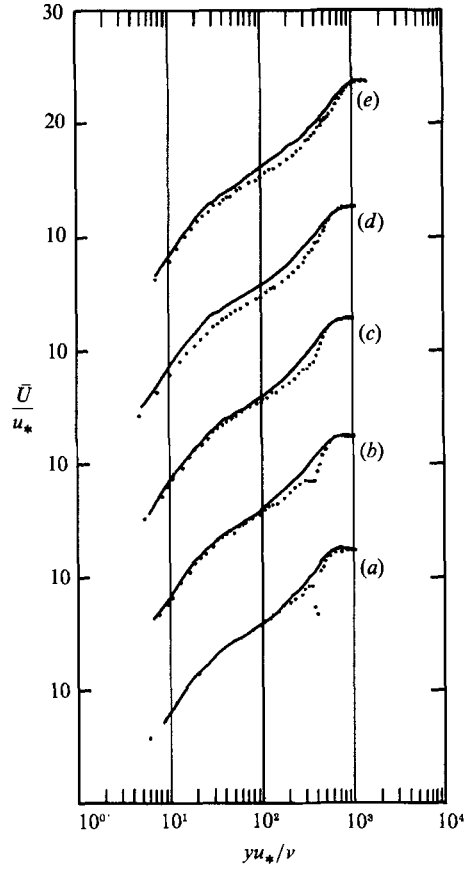

FIGURE 2. Distribution of $\bar{U}/u_*$ plotted against yu_*/ν. (*a*) $\xi = 7.8$, (*b*) 11.9, (*c*) 17.3. (*d*) 28.1, (*e*) 71.4 ——, Natural; · · ·, manipulated.

was found by minimizing a least-squares fit.† Spalding's formula is valid only in the wall region, hence only data below $y^+ = 200$ were used to determine u_*. This technique thus avoided the non-equilibrium portion of the profiles due to the manipulators' wake. When applied to the unmanipulated boundary layers, the value of u_* obtained from Coles' (1968) method always differed by less than 3% from that obtained by Spalding's law of the wall.

A comparison of the skin-friction coefficients for the natural and manipulated cases is shown in figure 3. (Other integral properties of the boundary layer are given by Chang 1987.) The skin-friction coefficient, C_f, was calculated from

$$C_f = 2(u_*/U_\infty)^2.$$

A maximum C_f reduction of about 15% in the manipulated case was found between $\xi \approx 30$–50. This result is comparable with those of Lemay *et al.* (1985), and Westphal (1986).

Figure 4 shows the streamwise r.m.s. velocity results obtained in the isothermal and heated boundary layer scaled with the outer variables, δ_n and U_∞, where δ_n is the

† This technique was also generalized to include an unknown offset, y_{off}, from the wall. However y^+_{off} was always found to be less than $0.5\nu/u_*$ indicating that the distance from the wall was well known *a priori*.

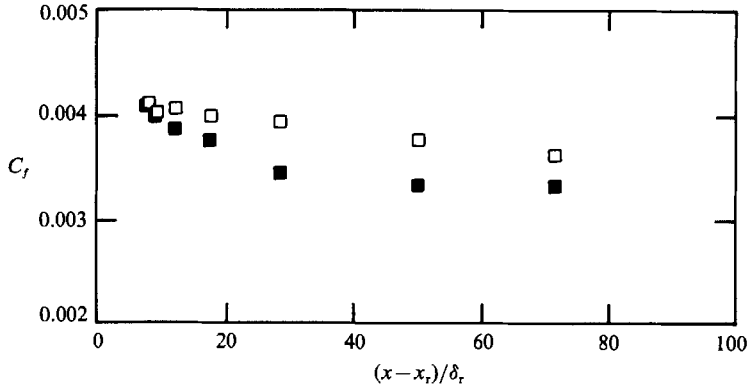

FIGURE 3. Skin-friction coefficient *vs.* the streamwise position. □, Natural; ■, manipulated.

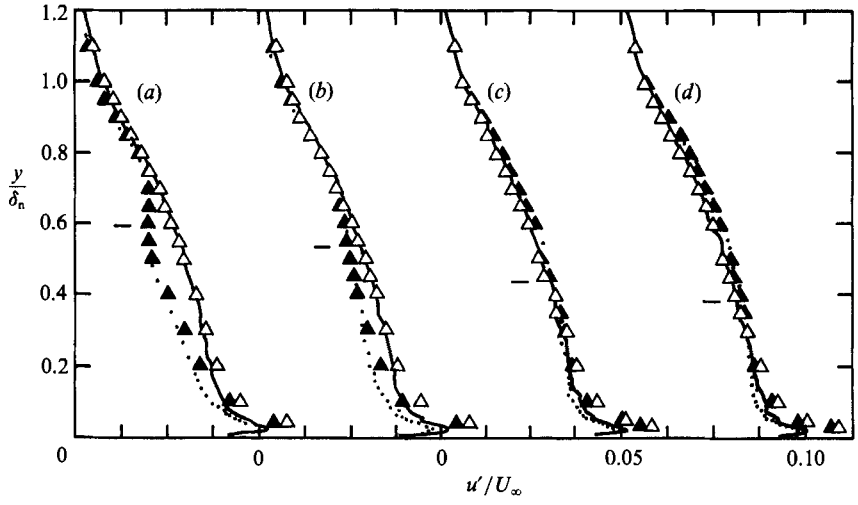

FIGURE 4. Distribution of u'/U_∞ plotted against y/δ_n. (*a*) $\xi = 17.3$, (*b*) 28.1, (*c*) 49.7, (*d*) 71.4. $\times$–θ wire results: △, natural; ▲, manipulated. Single wire results: ——, natural; · · ·, manipulated in the isothermal flow.

local boundary-layer thickness in the natural case. The velocity correction assumed for the $\times$–θ wire in a heated flow field is supported by the similarity of these two data sets. Immediately downstream of the manipulators, i.e. $\xi = 7.8$, Chang (1987) found a sharp increase in the u' intensity. This was due to the vortex shedding behind the manipulators. Its shedding frequency varied with the free-stream velocity and followed the $\frac{3}{2}$ power law as found by Sato & Kuriki (1961). Under the experimental conditions of a 5 m/s free-stream velocity, the shedding frequency was approximately 800 Hz and had disappeared at approximately $\xi = 10$ downstream according to Blackwelder & Chang (1986).

Figure 4 also shows that u' decreased at $\xi = 17.3$ with a maximum r.m.s. reduction of 30% at $y/\delta_n = 0.5$ ($y^+ = 340$) which is in the lower wake region of the boundary layer. Corke, Guezennec & Nagib (1980) speculated that the reduction of the u' intensity near the wall region would cause a decrease in the bursting rate near the wall. However, when the local u' or θ' was used for a threshold in the VITA or quadrant scheme, the bursting rate of the present data showed no significant difference in the near-wall region; i.e. less than 10% difference from the natural case.

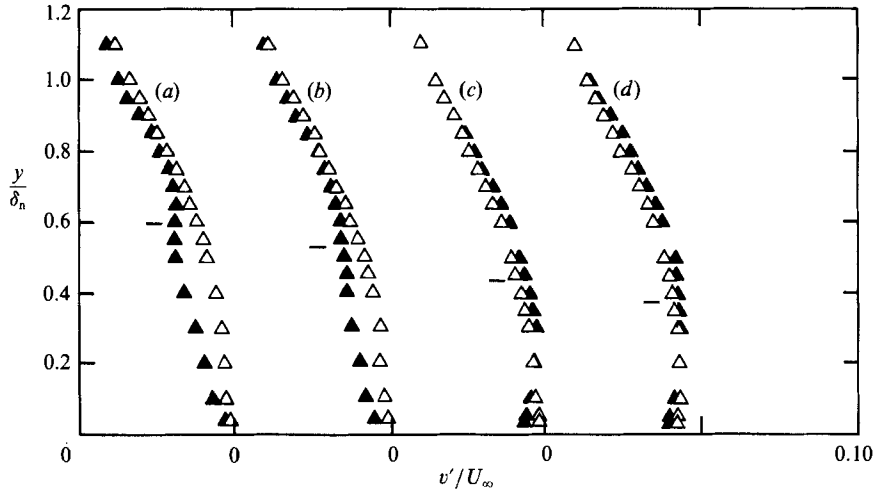

FIGURE 5. Distribution of v'/U_∞ plotted against y/δ_n. (*a*) $\xi = 17.3$, (*b*) 28.1, (*c*) 49.7, (*d*) 71.4. △, Natural; ▲, manipulated.

Downstream at $\xi \gtrsim 50$, the u' intensities had almost returned to the values in the natural case but with a slight overshoot in the outer layer. In this and subsequent figures, the short horizontal line to the left of the data is the elevation of the manipulator upstream.

The normal velocity intensity was similar to the streamwise velocity intensity and is shown in figure 5. The maximum reduction was about 25% at $y/\delta_n = 0.5$ and $\xi = 17.3$. This indicates that the vertical mixing was drastically inhibited by the manipulators, which agrees with Guezennec & Nagib (1985). Nevertheless, their result showed that at $\xi = 45$, the v' intensity was still recovering, while the u' intensity had relaxed back to the value in the natural case. In the present experiments, both u' and v' have reached their natural state at this distance. This result is similar to those of Lemay *et al.* (1987) up to $\xi = 30$ except for the lower value for the manipulated case near the wall in figure 5.

4.3. *Temperature measurements*

A line heater was placed $0.75\delta_r$ from the wall 1 mm directly behind the second manipulator. The input power was approximately 72 W as monitored by an ammeter and a voltmeter. The heating wire was vertical but the mixing was quite rapid; hence the buoyancy effects were small. The mean and r.m.s. temperature profiles at $\xi = 13.2$ are shown in figure 6. The manipulator and heater position are marked on the ordinate. The abscissa is the temperature in degrees Centigrade, where $\Theta(y,t) = \bar{\Theta}(y) + \theta(y,t)$ and $\theta(y,t) = T(y,t) - \bar{T}(y)$. When the manipulators were added, the mean temperature distribution was slightly narrower and the peak r.m.s magnitude decreased by 30–35% indicating that the temperature mixing was reduced. Additional data taken with the heater at $y = 0.52\delta_r$ indicated that the manipulators reduced the mixing in this case also as both the mean and r.m.s. temperatures in the outer region of the boundary layer were reduced. Figure 6 shows the same trend as the data of Bonnet, Delville & Lemay (1987) although they reported results for $1 < \xi < 7.5$ only.

The simultaneous temperature signals of the rake were also studied. Figure 7 shows both the natural and modified boundary-layer data. The temperature scale is

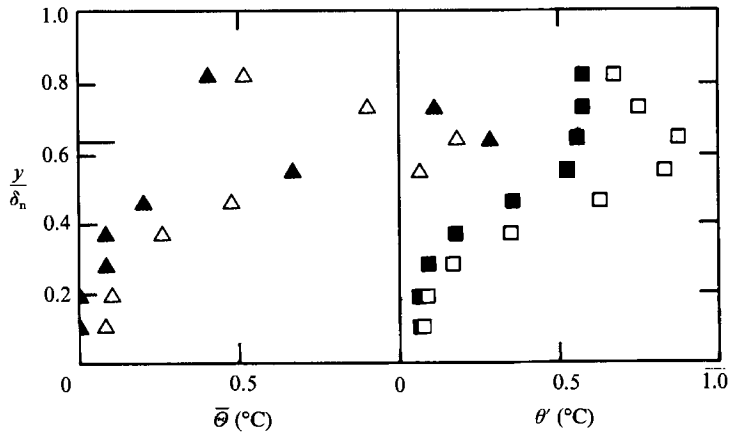

FIGURE 6. Distributions of temperature mean, $\bar{\Theta}$, and r.m.s., θ', plotted against y/δ_n at $\xi = 13.2$. The heater is placed at $0.75\delta_r$ and the data were measured in the low-turbulence wind tunnel. $\bar{\Theta}$: △, natural; ▲, manipulated. θ': □, natural; ■, manipulated.

given in the lower left-hand corner. The sensor positions are shown on the right-hand side in both inner and outer variables. The timescale in both dimensional and non-dimensional forms is given on the abscissa. The temperature amplitude fluctuations in the manipulators' wake region is strongly decreased and heated fluid in the lower region of the boundary layer is less frequently observed. In addition, when heat was added at $y = 0.52\delta_r$ (not shown), the temperature fluctuations were reduced in the outer wake region, i.e. $y \geqslant 0.6\delta_n$, suggesting that the manipulators had inhibited mixing across the layer. Furthermore, when heat was released in the logarithmic region at $y^+ = 75$, there was no significant difference between the natural and manipulated cases at $\xi = 13.2$, indicating that the effect of the manipulators was primarily felt further downstream.

Mean and r.m.s. temperatures were also obtained with the rake and the $\times$-θ wire in the boundary layer heated uniformly at the wall in the Dryden tunnel. Since both results were identical, only the $\times$-θ probe r.m.s. results are shown in figure 8 where $\Theta_w = \bar{T}_w - T_\infty$. It was found that the mean temperature had recovered to its natural case at $\xi \geqslant 50$, which is faster than the mean velocity recovery. As shown in figure 8, the r.m.s. temperature, θ', in the manipulated case was reduced by about 30% at $y/\delta_n = 0.8$ and $\xi = 17.3$. This amount of reduction was about the same order as the reductions of u' and v'; however, the location of the maximum reduction was different. In the r.m.s. velocity measurements, u' and v' were reduced most in the region near $y/\delta_n = 0.5$. In the temperature case, the strongest reduction occurred at $y/\delta_n \approx 0.8$. The r.m.s. temperature of the manipulated case also returned to its unmanipulated value after $\xi = 50$.

Figure 9 is a plot of simultaneous temperature signals from the rake at $\xi = 17.3$. The temperature scale is shown in the lower left-hand corner. The distance of the sensors from the wall is given on the right; the lowest position was $0.06\delta_n$ or 38 wall units and the outermost sensor was at $1.3\delta_n$. The time traces in both dimensional and non-dimensional forms are given on the abscissa. It was observed that the amplitudes of the temperature fluctuations in the manipulated case were strongly reduced in the manipulators' wake region. In addition, fluctuations in the temperature signals were seen to be less frequent in the outer region of the boundary layer. Simultaneous records of the temperature at ten spanwise locations also showed

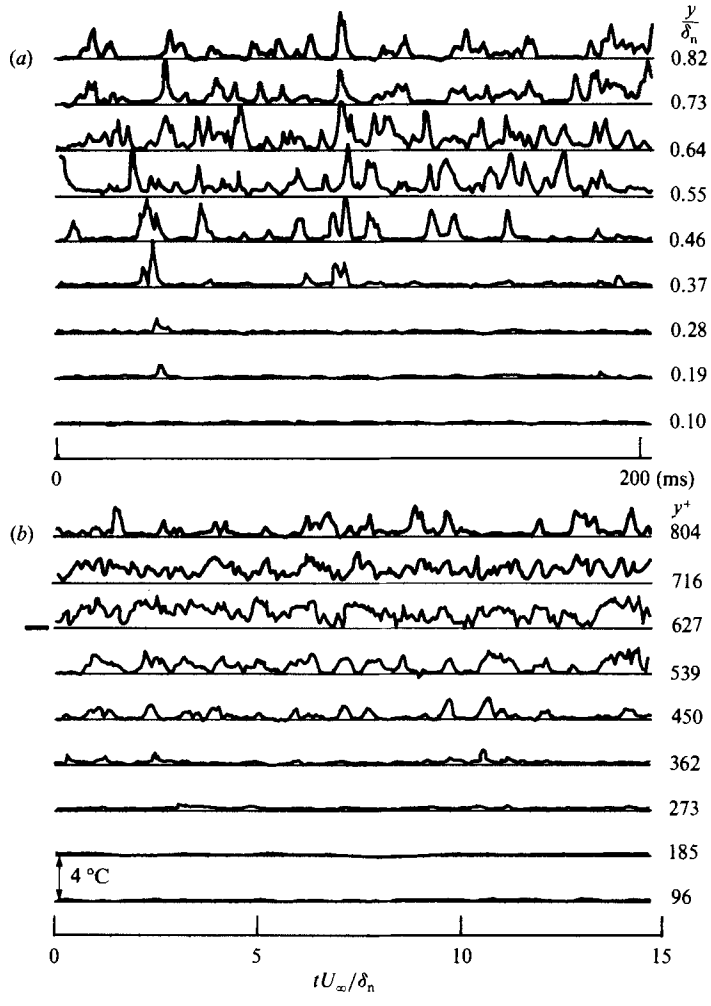

FIGURE 7. Simultaneous temperature signals, $\Theta(y,t)$, corresponding to figure 6. (*a*) Natural, (*b*) manipulated.

that, at $y \geqslant 0.8\delta$, the instantaneous signals were correlated over smaller spanwise distances in the manipulated boundary layer.

There were sharp temperature reductions, as described by Chen & Blackwelder (1978), crossing the boundary layer in both the natural and manipulated cases. Recorded data indicated that these sharp reductions were found less frequently in the manipulated case. Chen & Blackwelder (1978) used the coincidence correlation method, applying the VITA scheme and conditional averaging, to find the optimal time delay between each wire and then to portray this sharp rapid cooling in terms of a spatial configuration. When this particular method was applied to the natural and manipulated cases, it was found that there was no significant change in this relationship; the difference between the natural and manipulated sharp cooling was within the experimental scatter (i.e. less than $\pm 1.0\nu/u_*^2$).

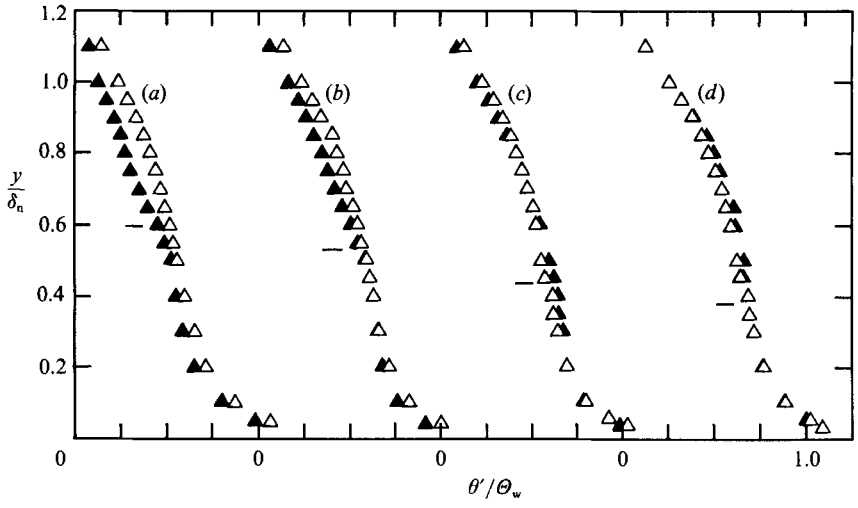

FIGURE 8. Distribution of θ'/Θ_w plotted against y/δ_n. (*a*) $\xi = 17.3$, (*b*) 28.1, (*c*) 49.7, (*d*) 71.4. △, Natural; ▲, manipulated.

4.4. *Reynolds stress and turbulent heat fluxes*

The Reynolds stress, and the turbulent heat fluxes in the streamwise and normal directions normalized with the local u', v' and θ' are shown in figures 10, 11 and 12. In the natural case, R_{uv} and $R_{v\theta}$ had small values near the wall in both the manipulated and natural boundary layers. $R_{u\theta}$ had a large value in this region, which indicates a strong correlation between the u- and θ-signals in both boundary layers. In the natural boundary layer, at $0.3 \leqslant y/\delta_n \leqslant 0.7$, R_{uv}, $R_{u\theta}$ and $R_{v\theta}$ were approximately constant with values of 0.42, 0.56 and 0.48 respectively. $R_{u\theta}$ and $R_{v\theta}$ agree well with Chen's values of 0.60 and 0.51, and although R_{uv} is different from Chen's 0.53, it does agree with the values commonly reported such as 0.44 found by Subramanian & Antonia (1981). Note that the temperature-corrected R_{uv} agreed well with previous unheated-wall values.

In the manipulated case, the correlation coefficients had a more complicated behaviour. The R_{uv} and $R_{u\theta}$ correlation values generally increased above the manipulators' position and decreased below. $R_{v\theta}$ remained relatively unchanged but showed a decrease at $y > 0.8\delta$. On the other hand, the raw values of these cross-products yield a different result. This is seen by examining the covariances in the manipulated layer normalized by the fluctuation magnitudes in the natural boundary layer. These values are called the modified Reynolds stress and turbulent heat fluxes, and are also plotted in figures 10–12. It is evident that the cross-products decreased almost everywhere for $\xi \lesssim 50$; the only exception being R_{uv} at $0.7 < y/\delta < 0.9$. Further downstream, the modified coefficients are slightly larger than the natural values at $y > 0.3\delta$, i.e. in the wake region of the boundary layer, and are slightly smaller near to the wall.

4.5. *Length scales; Taylor microscale*

The Taylor microscale for the velocity and temperature were measured by using the temporal derivative of the signal and Taylor's hypothesis. Both scales were typically 0.1δ in the natural boundary layer. In the manipulated flow, the microscales were reduced immediately behind the manipulators, but relaxed back to their un-

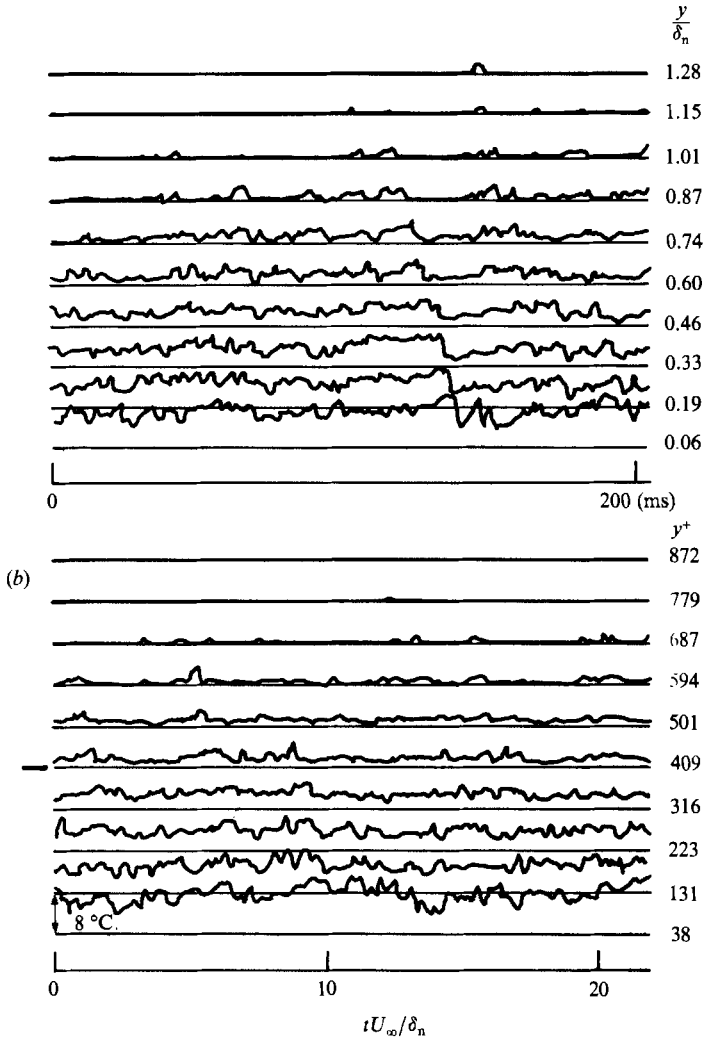

FIGURE 9. Simultaneous temperature signals, $\Theta(y,t)$, in the normal direction at $\xi = 17.3$. (*a*) Natural, (*b*) manipulated.

manipulated values by $\xi = 25$. Thus, the influence of the manipulators on this scale was confined to their immediate wake region. These results agree with the previous work of Blackwelder & Chang (1986). They found that at $\xi < 10\delta_r$ the manipulators' wake was dominated by vortex shedding with a frequency of about 800 Hz that was Reynolds-number dependent. Also the most unstable wavelength was approximately $4\pi(l\nu/U_\infty)^{\frac{1}{2}}$ as suggested by Sato & Kuriki (1961) and was comparable with the Taylor microscale.

The integral lengthscales associated with the velocity and temperature were computed by integrating the autocorrelation functions to their first zero crossing using Taylor's hypothesis. The results of the velocity measurements are shown in figure 13. The lengthscale and normal distance are scaled with the local natural boundary-layer thickness. It is apparent that the velocity integral lengthscale was substantially reduced in the boundary layer by the manipulators and this reduction persisted in the streamwise direction. The most significant difference appeared at

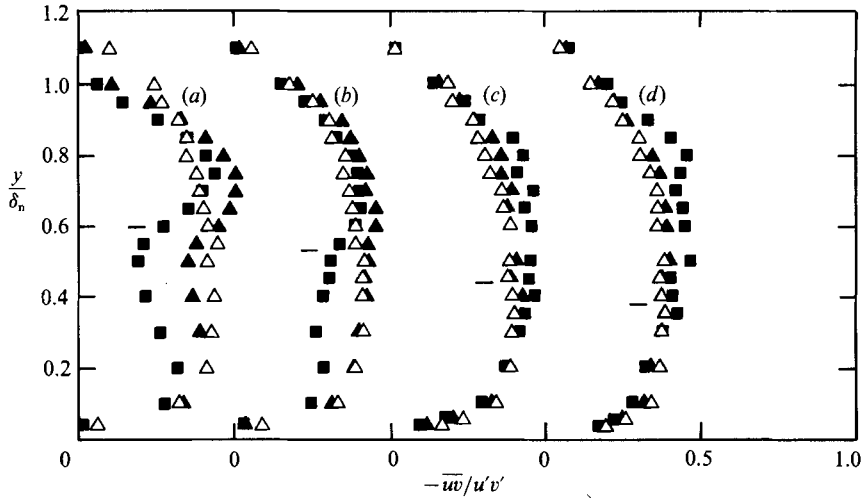

FIGURE 10. Distribution of $-\overline{uv}/u'v'$ plotted against y/δ_n. (*a*) $\xi = 17.3$, (*b*) 28.1, (*c*) 49.7, (*d*) 71.4. △, Natural; ▲, manipulated; ■, modified.

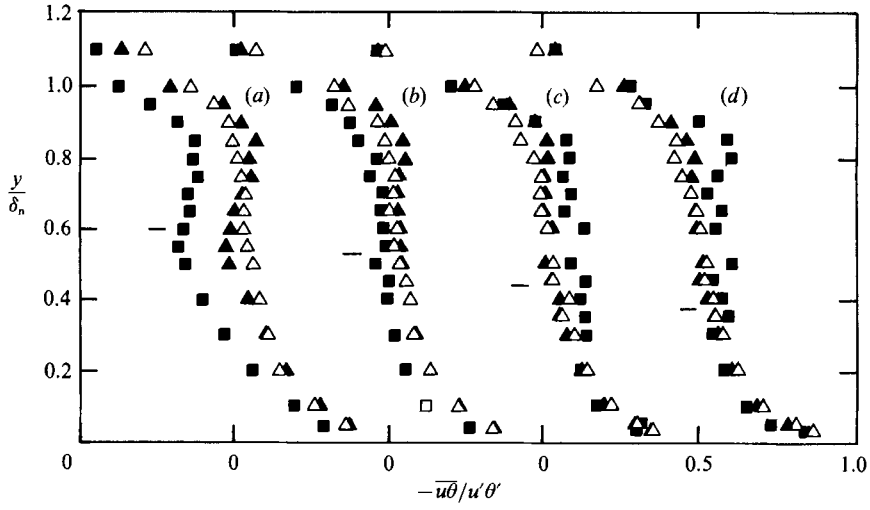

FIGURE 11. Distribution of $-\overline{u\theta}/u'\theta'$ plotted against y/δ_n. (*a*) $\xi = 17.3$, (*b*) 28.1, (*c*) 49.7, (*d*) 71.4. △, Natural; ▲, manipulated; ■, modified.

$y/\delta_n = 0.8$ and $\xi = 17.3$, where a 35–40% reduction was found. Downstream, the reduction became smaller but the effect spread to the entire boundary layer. At $\xi =$ 71.4 a 10% reduction can still be noted across most of the layer. It is not clear if the modified large-scale eddies were still recovering to the natural case or had reached another asymptotically stable state. Contrary to the Taylor microscale results, which showed that the reduction was confined to and associated with the manipulators' wake region only, the integral lengthscale results indicated that the range of this large-scale eddy reduction was comparable with and exceeded the distance of maximum skin-friction coefficient reduction. This suggests that the drag reduction on the wall must be related to the modification of the large-scale structures in the outer region of the boundary layer. The reduction of the temperature integral

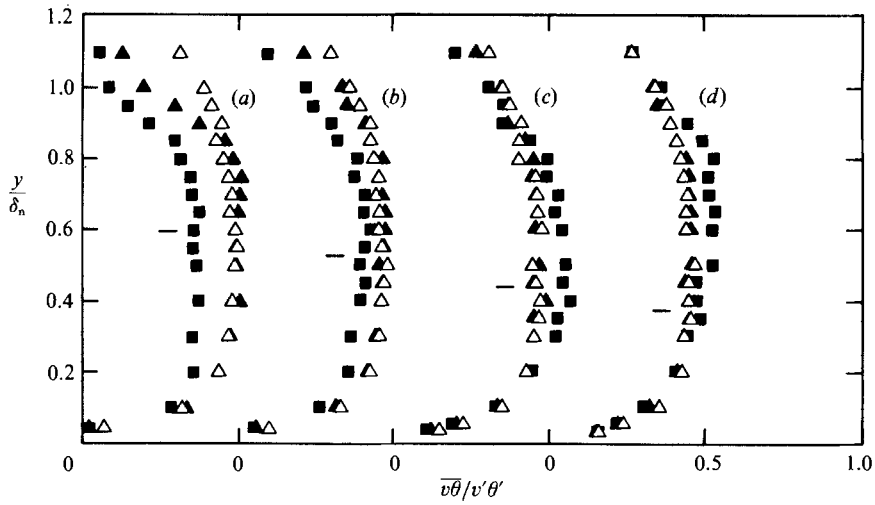

FIGURE 12. Distribution of $\overline{v\theta}/v'\theta'$ plotted against y/δ_n. (*a*) $\xi = 17.3$, (*b*) 28.1, (*c*) 49.7, (*d*) 71.4. △, Natural; ▲, manipulated; ■, modified.

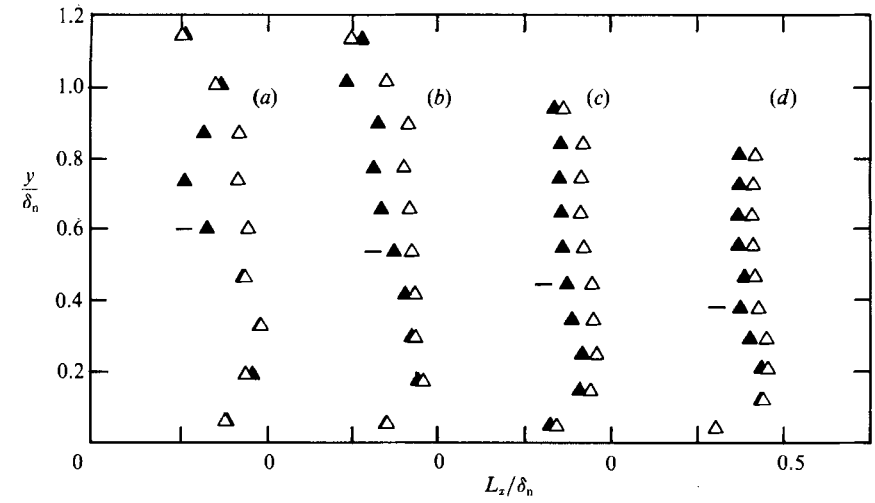

FIGURE 13. Distribution of streamwise velocity integral lengthscale, L_x/δ_n, plotted against y/δ_n. (*a*) $\xi = 17.3$, (*b*) 28.1, (*c*) 49.7, (*d*) 71.4. △, Natural; ▲, manipulated.

lengthscale was not as large as that in the velocity case; nevertheless, a broad influence could still be observed in the normal as well as streamwise directions.

4.6. *Space–time cross-correlations*

The space–time cross-correlation coefficient of two fluctuating signals, $p(t)$ and $q(t)$, is conventionally defined as

$$R_{pq}(X, Y, Z, T) = \frac{\overline{p(x_0, y_0, x_0, t_0)\, q(x, y, z, t_0+\tau)}}{p'q'},$$

where $p(t) = P(t) - \bar{P}$ and $q(t) = Q(t) - \bar{Q}$. The reference probe coordinates of signal $P(t)$ are x_0, y_0 and z_0, the correlated probe coordinates with signal $Q(t)$ are x, y and z. τ is the time delay between $P(t)$ and $Q(t)$. X, Y, Z and T are the spatial and temporal separations non-dimensionalized with δ_n and U_∞.

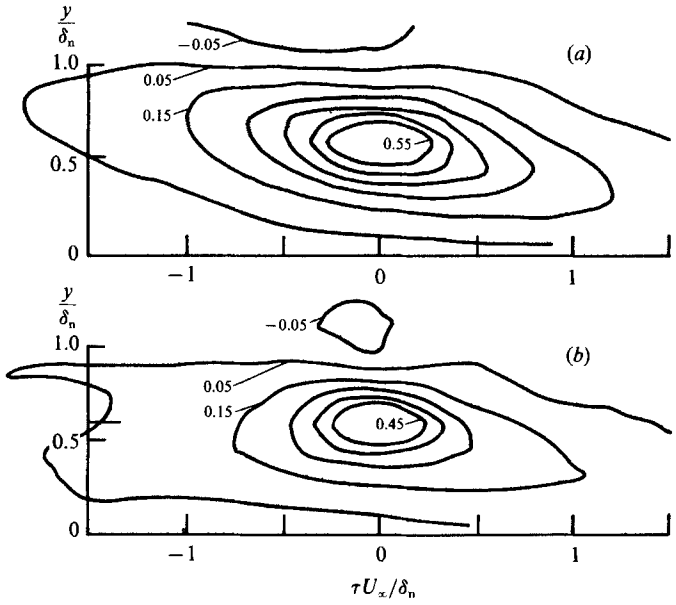

FIGURE 14. u-Component velocity cross-correlation maps in the normal direction at $\xi = 17.3$. (a) Natural, (b) manipulated.

The u-component velocity isocorrelation maps, $R_{uu}(0, Y, 0, T)$, are shown in figure 14 at the station $\xi = 17.3$. The reference probe was placed at $y_0 = 0.6\delta_n$. These velocity correlations are elongated in the streamwise and narrow in the normal directions, consistent with Kovasznay *et al.* (1970). Figure 14 indicates that the modified structures were significantly reduced. Based on the contour value of 0.15, the lengthscales are reduced by 20 and 30% in the y- and x-directions, respectively, comparable with the results of Lemay *et al.* (1987). This correlation also shows that the orientation of the structures, which in the natural case was about 10° with respect to the flow direction, was altered by the manipulators to be more parallel to the x-axis. The regions of negative correlations at $y \geqslant \delta_n$ are due to higher speed flow over the tops of the slower moving eddies and may be associated with the entrainment process of the interface. The reduction of the negative isocorrelation regions in figure 14 indicates that the large eddies and the entrainment process were altered by the manipulators. Isocorrelation maps of the temperature, $R_{\theta\theta}(0, Y, 0, T)$, indicated a similar but smaller change in the eddy structure; Chang (1987) found that the 0.15 contour was reduced by 12 and 23% in the y- and x-directions respectively.

The u-component correlations in the spanwise direction $R_{uu}(0, 0, Z, 0)$ at $y/\delta_n = 0.8$ are shown in figure 15. With the result in the previous figure, this suggests that the natural eddies of the velocity field were rather long in the mean flow direction and narrow in the cross-planes with a negative correlation located laterally at about $0.5\delta_n$. In the manipulated boundary layer, the size in the x- and z-directions was reduced. In addition, the region of negative correlation near $\Delta z \sim 0.5\delta_n$ disappeared completely, indicating that the large-eddy eruptions and/or the entrainment process is significantly altered by the manipulators. Similar reduction of lengthscales was also found in the spanwise temperature correlations.

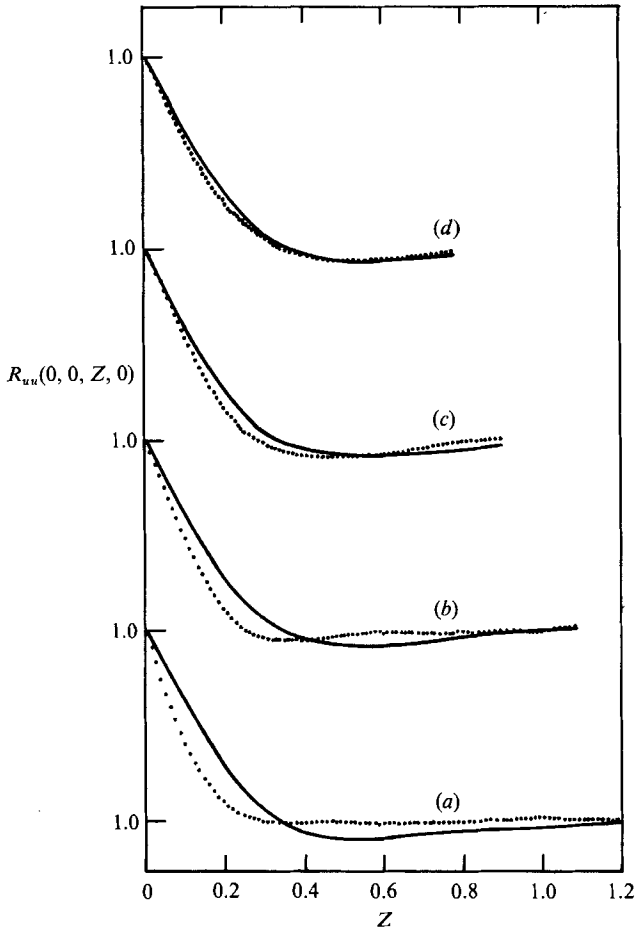

FIGURE 15. u-Component velocity cross-correlation coefficient, $R_{uu}(0,0,Z,0)$ at $y/\delta_n = 0.8$ and $\tau = 0$. ——, Natural; · · ·, manipulated. (*a*) $\xi = 17.3$, (*b*) 28.1, (*c*) 49.7, (*d*) 71.4.

4.7. *Conditional measurements*

The intermittency function, $\gamma(y)$, is defined as

$$\gamma(y) = \lim_{\Delta t \to \infty} \int_0^{\Delta t} I(y,t)\,\mathrm{d}t,$$

where $I(y,t)$ equals unity when the flow at y is turbulent and is zero otherwise. Corrsin & Kistler (1955) proposed the empirical relationship

$$\gamma(y) = 0.5\left[1 - \mathrm{erf}\left(\frac{y-\bar{Y}}{\sqrt{2}\sigma}\right)\right],$$

where

$$\mathrm{erf}(\chi) = \frac{2}{\pi^{\frac{1}{2}}}\int_0^{\chi} \mathrm{e}^{-\eta^2}\,\mathrm{d}\eta,$$

and $\bar{Y}$ and σ are the statistical mean position and standard deviation of the interface, respectively, obtained from the data. Figure 16 gives the measured intermittency in the boundary layer together with a least-squares fit of the data to the above

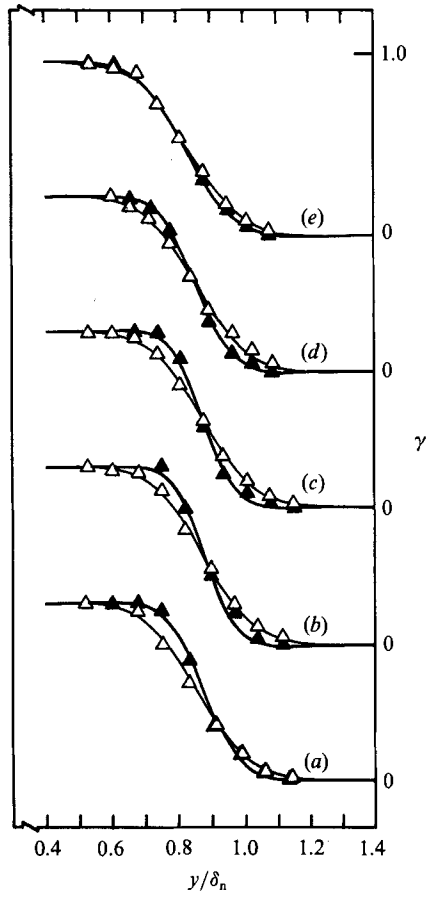

FIGURE 16. Distribution of the intermittency, γ, plotted against y/δ_n. The solid lines are the error functions obtained by a least-squares fit. (*a*) $\xi = 7.8$, (*b*) 11.9, (*c*) 17.3, (*d*) 28.1, (*e*) 71.4. △, Natural; ▲, manipulated.

relationship. The flow field near the manipulators, $\xi = 7.8$, showed an altered intermittency profile only in the region $0.65 < y/\delta < 0.85$. Further downstream, $\xi > 10$, the manipulators affected the intermittency everywhere and decreased the width of the intermittent region uniformly. The intermittency distributions had a maximum slope near $y/\delta_n \approx 0.85$. There was no apparent variation of γ in the spanwise direction, which agrees well with the spanwise uniformity results in the mean and r.m.s. quantities and the lengthscales.

The interface crossing frequency distribution is defined as the number of large turbulent eddies passing per unit time and was measured by the changes in $I(y,t)$ from zero to unity. It has been scaled with δ_n and U_∞ and plotted in figure 17. The solid lines are the Gaussian function proposed by Thomas (1973):

$$F(y) = \frac{C}{(2\pi)^{\frac{1}{2}}\sigma}\exp\left[-\left(\frac{y-\bar{Y}}{\sqrt{2}\sigma}\right)^2\right],$$

where C is a proportionality constant obtained by a least-squares fit of the natural and manipulated data. As shown in figure 17, the crossing frequency distribution with the manipulators had a sharper and narrower distribution everywhere

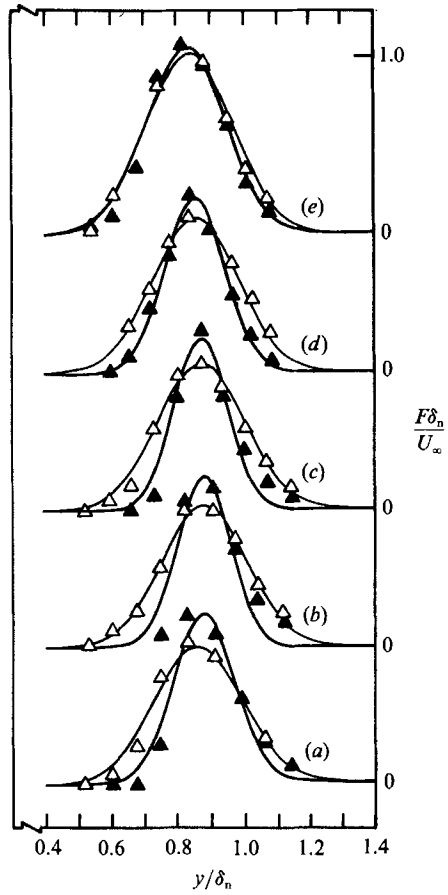

FIGURE 17. Distribution of the non-dimensional crossing frequency, $F\delta_n/U_\infty$ plotted against y/δ_n. The solid lines are Gaussian functions obtained by least-squares fits. (*a*) $\xi = 7.8$, (*b*) 11.9, (*c*) 17.3, (*d*) 28.1, (*e*) 71.4. △, Natural; ▲, manipulated.

downstream. The data show a slight positive skewness at the early stations, possibly due to the manipulators lying below the centre of the intermittent region. After $\xi =$ 17.3, the crossing frequency distribution of the manipulated case slowly approached the undisturbed state. The non-dimensional frequency, $F_m \delta_\eta/U_\infty$, where F_m is the frequency at $\gamma = 0.5$, increased as ξ increased for both the natural and the manipulated boundary layers. The frequency for the modified boundary layer was typically 15–20% higher, as seen in figure 17. The increase in the streamwise direction for the natural case may be a slight Reynolds-number effect.

Figure 18 indicates that $\bar{Y}/\delta_n$ and σ/δ_n in the natural case remain approximately constant in the ξ-direction. In the manipulated case $\bar{Y}/\delta_n$ had nominally the same value of 0.87 as in the natural case. This value is slightly higher than the 0.75 from Hedley & Keffer (1974*b*) and the 0.80 from Kovasznay *et al.* (1970) and Corrsin & Kistler (1955), but is closer to the 0.82 from Chen (1975). Note that Chen's measurements were based on temperature signals, and the others were velocity signals. The variation of these values may be due to the different detection methods.

Guezennec & Nagib (1985) measured the intermittency of the velocity field in the manipulated case. Their intermittency distributions, however, both in the natural and manipulated cases, showed a shift toward the wall as the flow moved

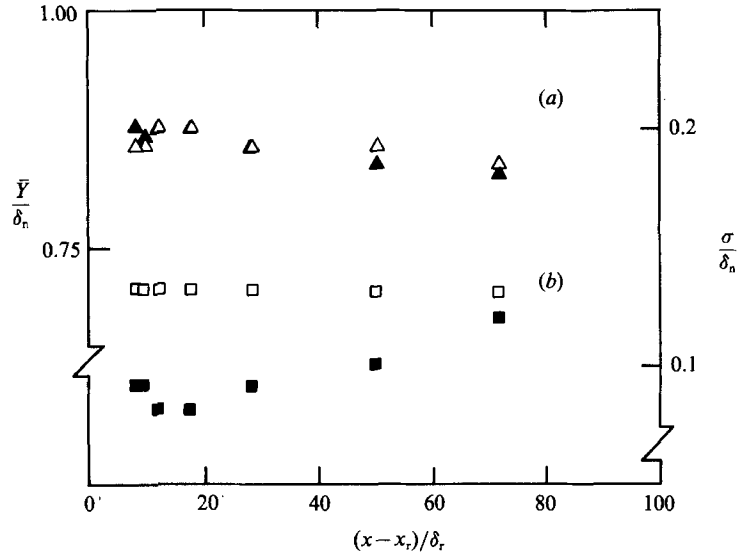

FIGURE 18. (*a*) Mean position of the interface $\bar{Y}/\delta_n$ and (*b*) standard deviation of the interface σ/δ_n, *vs.* the streamwise direction. △, □, Natural; ▲, ■, manipulated.

downstream, which differs from the present results. One difference between the two techniques is that they used velocity fluctuations, such as $(\partial u/\partial t)^2$ or $|uv|$, as the detection function. The threshold level and hold time were determined by matching the distribution and the associated timescales in the natural case with those results in Hedley & Keffer (1974*a*). Once these values were obtained, they were also applied in the manipulated case. Previous isocorrelation contour results, however, have shown that different normalization factors could result in different sizes of the structures. It is not clear whether or not the threshold level in the natural case should also be used in the manipulated boundary layer.

The standard deviation of the interface, σ/δ_n, in the natural case had a constant value of 0.13 in agreement with the value of 0.13 from Chen (1975), 0.14 from Corrsin & Kistler (1955), 0.15 from Kovasznay *et al.* (1970) and 0.24 from Hedley & Keffer (1974*b*). In the manipulated case, figure 18 indicates that σ/δ_n was reduced considerably at the upstream stations. This illustrates that the interface had a smaller amplitude and was less corrugated with the manipulators. The recovery of this manipulated interfacial structure was very slow. Since the entrainment is related to the distortion and excusion of the interface, the inference from this reduction of σ is that the entrainment was strongly inhibited by the manipulators.

Figure 19 shows the conditional zone averages of the streamwise velocity at $\xi =$ 17.3 in the form of a Clauser defect plot. The intermittency distributions in the natural and manipulated cases are also given as reference. The abscissa is the non-dimensional normal position, y, scaled with the natural boundary-layer thickness. The squares are the non-turbulent zone average of the streamwise velocity in the potential flow region, and the triangles are the turbulent zone average of the streamwise velocity inside the turbulent region. In the manipulated case, an obvious decrease in the turbulent and non-turbulent zone averages was found in the region of high intermittency.

Since the manipulators seemed to alter the intermittent region, it appeared that a scaling based upon the intermittent region, i.e. $\bar{Y}$ and σ, would present the data

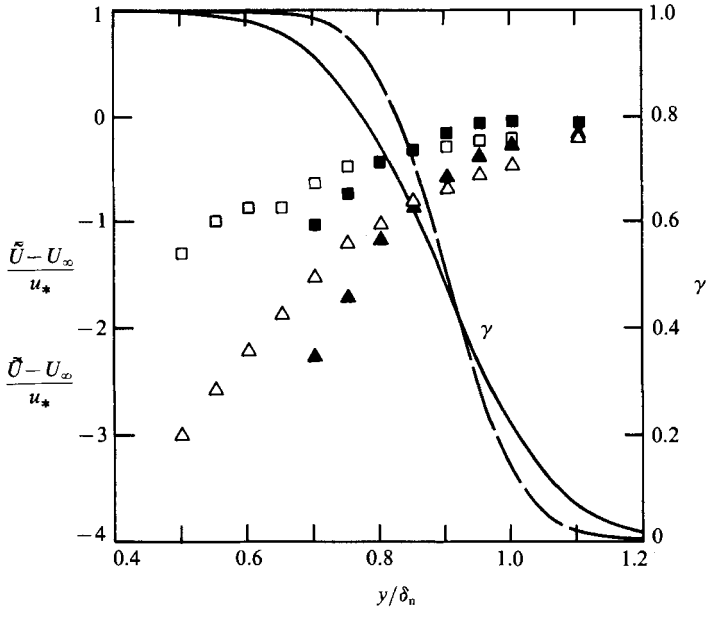

FIGURE 19. Zone averages of the streamwise velocity plotted against y/δ_n at $\xi = 17.3$. (The intermittency, γ, is given for reference: ——, natural; – – –, manipulated.) Turbulent zone average: △, natural; ▲, manipulated. Non-turbulent zone average: □, natural; ■, manipulated.

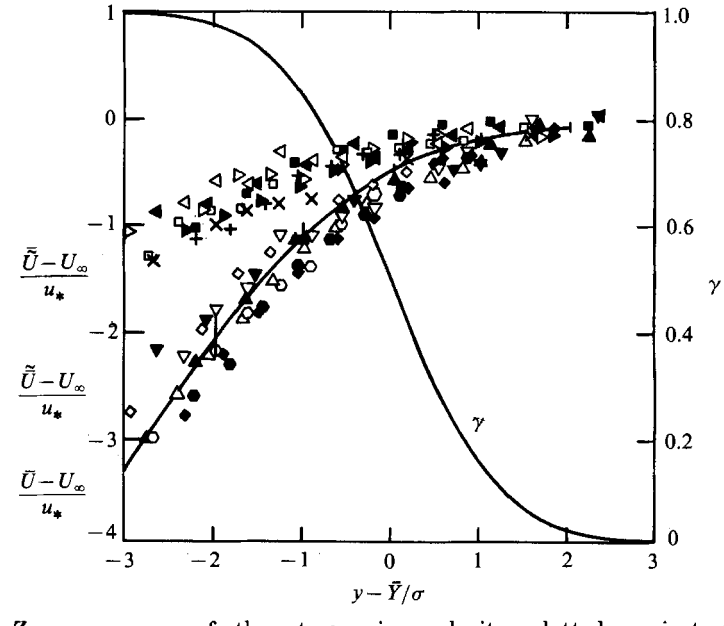

FIGURE 20. Zone averages of the streamwise velocity plotted against $(y-\bar{Y})/\sigma$. ——, Intermittency —+— mean with standard deviation. Turbulent zone averages at $\xi = 17.3$, 28.1, 49.7, 71.4: △, ▽, ◇, ○ natural; ▲, ▼, ◆, ● manipulated. Non-turbulent zone averages at $\xi = 17.3$, 28.1, 49.7, 71.4: □, ◁, ▷, ×, natural; ■, ◀, ▶, +, manipulated.

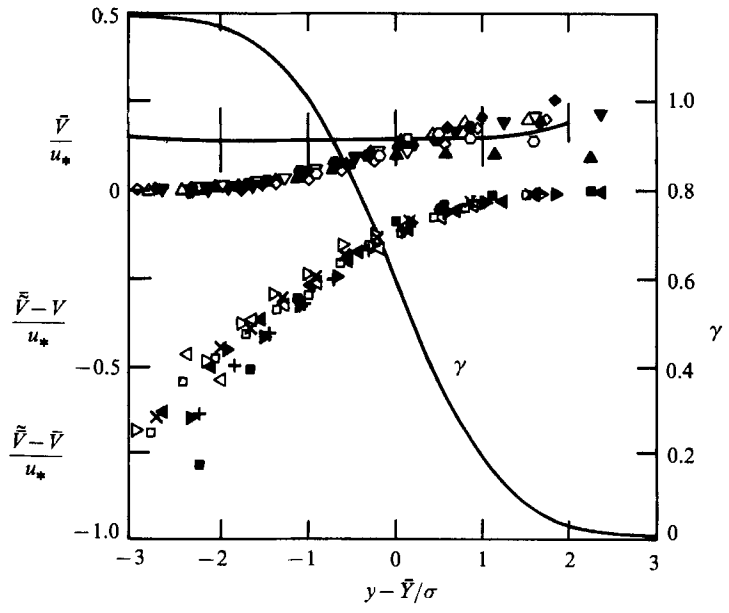

FIGURE 21. Zone averages of the normal velocity plotted against $(y-\bar{Y})/\sigma$. ——, Intermittency; —|— mean with standard deviation. Turbulent zone averages at $\xi = 17.3, 28.1, 49.7, 71.4$. △, ▽, ◇, ○ Natural; ▲, ▼, ◆, ● manipulated. Non-turbulent zone averages at $\xi = 17.3, 28.1, 49.7, 71.4$. □, ◁, ▷, ×, Natural; ■, ◀, ▶, +, manipulated.

better. This scaling is shown in figure 20 where the normal direction is measured from the centre of the intermittency region, $\bar{Y}$, and scaled with the width of the region, σ. The intermittency distributions of all the natural and manipulated cases are coincident. The solid line with bars in the figure is the mean velocity profile. The maximum difference between the non-turbulent and turbulent zone averages was about $2u_*$ at $(y-\bar{Y})/\sigma = -3$. One of the main conclusions of this research is that the interfacial scaling, $\bar{Y}$ and σ, provided a much better collapse of the data and thus showed that the manipulators left a boundary layer with smaller standard deviation, σ.

The conditional zone averages of the normal velocity, from which the local mean, $\bar{V}$, was subtracted, are shown in figure 21. The upper data points are the turbulent zone average, $(\tilde{\bar{V}}-\bar{V})/u_*$. Beyond the mean interface position, $(y-\bar{Y})/\sigma > 0$, $(\tilde{\bar{V}}-\bar{V})/u_*$ was slightly positive, which is consistent with the outward movement of the turbulent eddies. The lower data points are the non-turbulent zone average, $(\tilde{\bar{V}}-\bar{V})/u_*$. The negative sign shows that the irrotational fluid was approaching the wall with a much stronger velocity from the mean $\bar{V}$. Near the valley of the interface, $\tilde{\bar{V}}-\bar{V}$ was about $0.7u_*$ or $0.03U_\infty$. This is quite consistent with values found by Kovasznay *et al.* (1970) and Hedley & Keffer (1974*b*) in a natural boundary layer.

5. Summary and conclusions

In the present study the dynamical structural differences between the natural and manipulated boundary layers in a zero-pressure-gradient environment have been investigated. Experiments were performed to measure both the velocity and the temperature field. The wall was uniformly heated to 15 K above the ambient temperature and additional data with a line heater were also obtained.

The primary conclusion from this investigation is that the manipulators reduced the mixing in the wake region of the turbulent boundary layer. Heat released in the initial wake regions showed that the manipulators decreased the temperature intensity by a maximum of approximately 30–35%. Heat released in the lower wake region of the boundary layer was prevented from crossing through the manipulators' wakes and hence the mean and r.m.s. temperatures were both reduced in the outer region of the boundary layer. The mean temperature profiles had a sharper peak and greater magnitude in the presence of the manipulators, i.e. the manipulators had decreased the mixing in the wake region of the boundary layer.

The skin friction was reduced by 15% between $\xi = 30$ and 50 in agreement with Westphal (1986). The maximum reductions of the fluctuations in u, v, and θ were all about 30% at $\xi = 17.3$. However, the positions of greatest reduction were not the same; namely u' and v' had their maximum reduction at $y/\delta \approx 0.5$, while θ' had its maximum decrease at $y/\delta \approx 0.8$. The manipulators inhibit the mixing and decrease the fluid interchange between the wall region and outer region of the boundary layer. Consequently the heat added at the wall does not mix as much with the outer fluid and hence the temperature fluctuations decreased more in the outer region. Conversely the velocity differences associated with entrainment do not mix as well in the presence of the manipulators and thus the maximum velocity reduction should occur beneath the location of the manipulators, as was found. The reduction of the Taylor microscale was associated with the manipulators' near-wake region only. The maximum reduction was 15–20% at $\xi = 17.3$.

The velocity integral lengthscale was reduced by the manipulators as shown previously by spectral measurements of Coustols *et al.* (1987) near the manipulators and by Lemay *et al.* (1987) up to $\xi = 30$ downstream. The present results indicate that the integral lengthscale is the only variable that still showed a significant difference from the natural boundary-layer results at $\xi = 71.4$. This distance was comparable with the range of the skin-friction reduction and suggests that the reduction in the wall activity was due to the modification of the outer large-scale structures. The maximum reduction of the temperature integral lengthscale, about 10%, was less than that of the velocity integral scale, of 35–40%. Isocorrelation contours indicated that the temperature eddy structure in the normal direction was generally smaller than the velocity eddy structure and was less affected by the manipulators. The orientation of the temperature structures appeared unchanged. The temperature isocorrelation maps showed that the eddy size was reduced by approximately 10% in both the streamwise and normal directions. However, the reduction of the velocity isocorrelations was 20% in the streamwise direction and 15% in the normal direction. In addition the velocity correlations in the spanwise direction showed that the region of negative correlation in the natural case disappeared in the manipulated case, indicating again that entrainment was reduced.

A detection method based upon the temperature signal was used in both the natural and manipulated cases. It used the modified asymptotic ambient temperature as the threshold level to measure the interfacial properties of the natural and manipulated cases. It provided a sharper demarcation between the turbulent and non-turbulent fluid and led to the following results. The non-dimensional mean position of the interface for both the natural and manipulated cases was approximately $0.85\delta_n$–$0.87\delta_n$. The non-dimensional standard deviation of the interface was dramatically reduced by the manipulators. In the natural case, it had a constant value of about $0.13\delta_n$, but in the manipulated case a 40% reduction in σ occurred at $\xi = 17.3$. This strongly indicates that the entrainment was reduced. The

conditional turbulent and non-turbulent zone averages indicate that the proper scaling was with the interfacial coordinates, i.e. the mean and standard deviation of the interface position. The conditional averages of the Reynolds stress and heat fluxes in the non-turbulent region were small. Most of the Reynolds stress and heat fluxes were carried by the turbulent region.

The large-scale eddies in the outer region of the boundary layer are related to and govern the entrainment of the irrotational fluid into the boundary layer. Kovasznay *et al.* (1970) found that the normal velocity between these eddies was quite large, as exemplified by figure 21 of the present results. Chen & Blackwelder (1978) showed that the eddies in the outer region were related to the near-wall layer by a strong shear layer aligned with the backs of the outer eddies and extending to the wall. However, the present research found that this shear layer was not modified by the manipulators and consequently could not explain the drag reduction caused by the manipulators in the outer region. However, the manipulators did significantly decrease the lengthscales associated with the outer eddies and reduce the entrainment into the boundary layer as shown by the reduced excursions of the interface.

It appears that manipulators promote drag reduction indirectly by decreasing the growth of the boundary layer. That is, the temperature tagging showed that the mixing was strongly decreased. Consequently, the entrainment is reduced and the boundary layer grows less rapidly, which reduces the drag via the momentum theorem. From this point of view, the reported drag reduction is a result of reduced entrainment. This idea would explain why the optimal values of the manipulator's location, h/δ_r, as reported by Savill & Mumford (1988) and Lemay *et al.* (1985) has been found to be in the intermittent region of the boundary layer where entrainment primarily occurs. This result is supported by the similar trends of the data for the standard deviation of the interface compared with the local values of the skin friction reported by Westphal (1986) and Savill & Mumford (1988). In addition, this result suggests that the manipulators would not decrease the drag in internal flows because entrainment is non-existent. Such results have been recently reported by Prabhu *et al.* (1988) in a turbulent channel flow.

The authors thank Ian McLean for the measurements in the near wake of the manipulators. This research was sponsored by the Air Force Office of Scientific Research under contract number F49620-85-C-0080 monitored by James McMichael. Their support is gratefully acknowledged.

REFERENCES

ANDERS, J. B. 1985 *Aerospace Technology Conference and Exposition, Long Beach, California, SAE Tech. Paper Series* 861769.

ANDERS, J. B. 1989 *AIAA*-89-1011.

ANTONIA, R. A., BROWNE, L. W. B. & CHAMBERS, A. J. 1981 *Rev. Sci. Instrum.* **52**, 1382.

ANTONIA, R. A., DANH, H. Q. & PRABHU, A. 1977 *J. Fluid Mech.* **80**, 153.

BLACKWELDER, R. F. & CHANG, S.-I. 1986 *AIAA*-86-0287.

BLACKWELDER, R. F. & HARITONIDIS, H. 1983 *J. Fluid Mech.* **132**, 87.

BLACKWELDER, R. F. & KAPLAN, R. E. 1976 *J. Fluid Mech.* **76**, 89.

BONNET, J. P., DELVILLE, J. & LEMAY, J. 1987 In *Proc. RAeS Intl Conf. Turbulent Drag Reduction by Passive Means, London*, p. 45.

CHAMPAGNE, F. H. 1978 In *Dynamics Measurements in Unsteady Flows* (ed. L. S. G. Kovasznay), p. 101. Dynamic Flow Conference, Skovlunde, Denmark.

CHANG, S.-I. 1987 Modification of large eddies in a turbulent boundary layer. Ph.D. dissertation, University of Southern California.

CHEN, C.-H. P. 1975 The large scale motion in a turbulent boundary layer. Ph.D. dissertation, University of Southern California.

CHEN, C.-H. P. & BLACKWELDER, R. F. 1978 *J. Fluid Mech.* **89**, 1.

COLES, D. 1968 In *Proc. Computation of Turbulent Boundary Layer*, Vol. 1, p. 1. Stanford Conference.

CORKE, T. C., GUEZENNEC, Y. & NAGIB, H. M. 1980 In *Proc. Viscous Drag Reduction Symposium, Dallas. AIAA*, Vol. 72, p. 128.

CORRSIN, S. 1949 *NACA Tech. Note* 1864.

CORRSIN, S. & KISTLER, A. L. 1955 *NACA Rep.* 1244.

COUSTOLS, E., COUSTEIX, J. & BELANGER, J. 1987 In *Proc. RAeS Intl Conf. Turbulent Drag Reduction by Passive Means, London*, p. 250.

FIEDLER, H. 1978 In *Dynamics Measurements in Unsteady Flows* (ed. L. S. G. Kovasznay), p. 81. Dynamic Flow Conference, Skovlunde, Denmark.

GUEZENNEC, Y. G. & NAGIB, H. M. 1985 *AIAA*-85-0519.

GUTMARK, E. & BLACKWELDER, R. F. 1987 *Exp. Fluids* **5**, 217.

HEDLEY, T. B. & KEFFER, J. F. 1974*a* *J. Fluid Mech.* **64**, 625.

HEDLEY, T. B. & KEFFER, J. F. 1974*b* *J. Fluid Mech.* **64**, 645.

KOVASZNAY, L. S. G., KIBENS, V. & BLACKWELDER, R. F. 1970 *J. Fluid Mech.* **41**, 283.

LARUE, J. C. 1974 *Phys. Fluids* **17**, 1513.

LEMAY, J., PROVENCAL, D., GOURDEAU, R., NGUYEN, V. D. & DICKINSON, J. 1985 *AIAA*-85-0521.

LEMAY, J., SAVILL, A. M., BONNET, J.-P. & DELVILLE, J. 1987 In *Proc. 6th Turbulent Shear Flows Symposium, Toulouse*. Springer.

PLESNIAK, M. W. & NABIG, H. M. 1985 *AIAA*-85-0518.

PRABHU, A., VASUDEVAN, B., KAILASNATH, P. K., KULKARNI, R. S. & NARASIMHA, R. 1988 *Turbulence Management and Relaminerization, Heidelberg*, p. 97. Springer.

SATO, H. & KURIKI, K. 1961 *J. Fluid Mech.* **11**, 321.

SAVILL, A. M. & MUMFORD, J. C. 1988 *J. Fluid Mech.* **191**, 389.

SAVILL, A. M., TRUONG, T. V. & RYHMING, I. L. 1988 *J. Méc. Théor. Appl.* **7**, 353.

SCHUBAUER, G. B. & SKRAMSTAD, H. K. 1948 *NACA Rep.* 909.

SPALDING, D. B. 1961 *Trans. ASME* E: *J. Appl. Mech.* **28**, 455.

SUBRAMANIAN, C. S. & ANTONIA, R. A. 1981 *Intl J. Heat Mass Transfer* **24**, 1833.

THOMAS, R. M. 1973 *J. Fluid Mech.* **57**, 549.

WESTPHAL, R. V. 1986 *AIAA*-86-0283.